Tellus (1988), 40A, 107–119

Eigenstructure of eddy microfronts

By L. MAHRT and H. FRANK,* Department of Atmospheric Sciences, Oregon State University, Corvallis, Oregon 97331, USA

(Manuscript received September 2, 1986; in final form March 18, 1987)

ABSTRACT

Aircraft measurements of strong turbulence in a bora flow and in weak intermittent turbulence near the top of a nocturnal surface inversion layer are examined. An important feature of both types of turbulence are narrow zones of sharp gradients of velocity and temperature. These concentrated gradients, which are referred to as fronts in laboratory turbulence, are studied here by applying conditional sampling criteria and analyzing the eigenvectors of the resulting lagged multivariate covariance matrix. In addition, a new technique is developed which specifies a weighting function instead of specific selection criteria with cutoff values. The mathematics derived for the new technique leads to the usual eigenvalue problem for principal components except that the covariance matrix becomes transformed.

The above analyses indicate that the eddy microfronts seem to be related to the relative horizontal motion of the drafts generated by vertical motions in shear flows. The horizontal gradients are sharpest at the upstream edge of the drafts where convergence occurs between the horizontal motion of the draft and the horizontal motion of the ambient air. For strong turbulence, the eigenstructures identify several stages of eddy transport consistent with shear-driven overturning and transverse vorticity. For intermittent turbulence in strongly stratified flow, the eigen structures indicate the predominance of two-dimensional modes which coexist with overturning eddies and gravity wave modes.

1. Introduction

The nature of coherent structures in turbulence in stratified and near-neutral geophysical flows is poorly known. This situation contrasts with heated boundary layers where transport is often organized by thermals, or, laboratory flows where organization of eddies is often triggered by the geometry of the laboratory configuration and perhaps encouraged by low Reynolds number. However, a widely accepted viewpoint is that turbulence, in general, consists of coherent structures which organize development of smaller scale more chaotic motions.

The laboratory studies conducted by Gibson et al. (1968), Kim et al. (1971), Laufer (1975), Brown and Thomas (1977), Chen and Blackwelder (1978) and others indicate that the coherent structures, or main eddies, have well-defined sharp edges characterized by concentrated shear and temperature gradients. These zones are sometimes referred to as fronts, backs, microfronts or gust fronts. The concept of concentrated shear zones contrast with Townsend's (1976) concept of smooth eddies which can be represented in terms of trignometric and exponential functions.

Eddy microfronts have been studied extensively in the heated atmospheric surface layer and in laboratory flows where they are often identified in terms of a ramp or sawtooth temperature signal (Antonia and Van Atta, 1978; Antonia et al., 1979; Schols, 1984; and others). In the atmospheric surface layer, the ramp structures are generally thought to be edges of shear-modified, buoyancy-driven thermals although a few studies have suggested that such thermal

* Present address: Meteorologisches Institut, Universitat Karlsruhe 7500 Karlsruhe, West Germany.

elements and microfront edges are driven primarily by shear and associated pressure fluctuations (Schols and Wartena, 1986). The composite structure of wind gusts constructed in Panofsky and Dutton (1984, Fig. 12.6) also shows a ramp structure for the horizontal wind.

The asymmetry and associated microfronts of the ramp structures appear to be associated with relative horizontal motions induced by vertical drafts in the presence of vertical mean wind shear. Horizontal convergence due to the relative horizontal motion of the drafts may be responsible for the most important intensification of local horizontal gradients and formation of the eddy microfronts. Vortex stretching due to the mean strain rate or that induced by ambient eddies may provide additional convergence. Vortex stretching due to buoyancy accelerations was thought to maintain the sharp boundaries of thermals in the study of Kaimal and Businger (1970). The maintenance of sharp gradients is opposed by dynamic instability of the shear zones and diffusion by smaller scale turbulence.

Eddy fronts corresponding to sharp horizontal gradients are dominant features of the aircraft-measured turbulence in stratified atmospheric flow studied here. Such microfronts will serve as the focal point of our analysis. Since the gradients are sharpest on the convergence side of the drafts, the shape of the draft structures in the time series is often similar to asymmetric top hats. Examples of such structures in the data analyzed here are evident in time series plots in Mahrt (1985) and Mahrt and Gamage (1987).

We will begin examination of the structure of eddy frontal zones with traditional conditional sampling. Conditional sampling has been used to study coherent structures in laboratory turbulence (e.g., Chen and Blackwelder, 1978), in heated atmospheric boundary layers (e.g., Wilczak, 1984) and in atmospheric surface layers (e.g., Schols, 1984). The selected samples may contain different structural modes in which case the composited structure can be misleading. As a result we will analyze the eigenvectors of the lagged multivariate covariance matrix associated with the conditionally selected samples, similar to the methodology of Petersen (1976) and Panofsky and Dutton (1984).

Unfortunately, conditional sampling requires a degree of advance knowledge about the coherent structures and the results of such sampling may be sensitive to the sampling criteria. In the study of well-defined laboratory eddies of Blackwelder and Kaplan (1976), the composited results were found to be relatively insensitive to the sampling criteria. However, Greenhut and Khalsa (1982) found significant sensitivity to sampling cutoff criteria even in relatively simple atmospheric boundary layers. The turbulence studied here is complicated by strong intermittency and the nature of the most coherent structures are not known with confidence. Therefore, a second method will be developed for the computation of the eigenvectors which does not require selection criteria in the normal sense. With the new method, the derivation of the eigenvectors employs a weighting function.

While less knowledge of the nature of the main structures is required to initiate this analysis, the features resulting from use of the weighting function are less distinct. In the present study, structures which are produced by both the conditional sampling and use of continuous weighting will be considered more robust than those calculations produced by only one of the techniques.

2. Weighted eigenvectors

In this section, we derive the mathematics for the weighted eigenfunction calculations. Consider the multivariate observational vector

$$\mathbf{f}(z, x),$$

where z identifies the realization or sample and x indicates the relative position within the realization. In general, z could represent a three-dimensional position vector or could represent time or any other index which systematically identifies the different realizations. For example, z might indicate the time of the realization while x represents the position within the spatial domain upon which each sample is measured. In the analyses of Sections 5, 6, z is the position of each sample of horizontal structure extracted within the aircraft record while x is the relative position within each sample (Fig. 1a).

To study such structures, we wish to compute a function $\phi(x)$ which possesses maximum similarity to the realizations of $\mathbf{f}(z, x)$. More specifi-

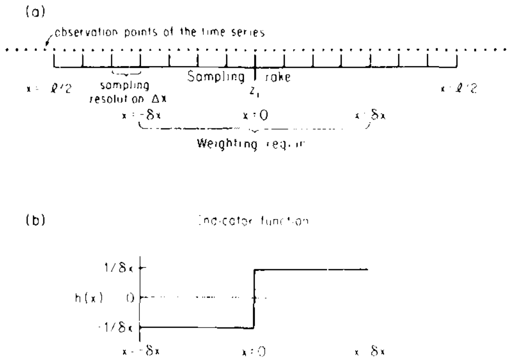

Fig. 1. (a) Geometry of sampling rake sequentially moved through a time series of discrete observations (dots). In this example only every third point is used. To generate samples the rake may be moved only one point or an arbitrary fixed number of points at a time. x is the relative position within the sample of width l. The sample is centered at point z_i of the time series. The weighting function is applied to a subregion of the sample rake of width $2\delta x$. (b) The step function indicator function (9) applied to the sample subregion of width $2\delta x$.

cally, a quadratic measure of similarity is defined as (e.g., Lumley, 1970; Busch and Petersen, 1971; Panofsky and Dutton, 1984)

$$\rho^2(z) = \left[\int_0^l f(z,x)\phi(x)\,\mathrm{d}x\right]^2 \Big/ \int_0^l \phi^2(x)\,\mathrm{d}x, \tag{1}$$

where l is the domain of the realization located at z. In the usual eigenvector approach, $\rho^2(z)$ is maximized over a finite number of observed samples in which case z takes on discrete values.

Samples are usually selected by specifying conditional sampling criteria. Selection of all possible samples from a stationary time series leads to loss of phase information and degeneracy of the eigenvalue-problem as discussed in Section 3. This loss of phase information can be restored without specifying selection procedures through use of a continuous weighting function. Examples of determination of the weighting function are presented in the next section.

One then wishes to maximize the expected value of the similarity measure (1) subject to the specified weighting function $g(z)$; that is, we wish to maximize

$$\lambda = E[g(z)\rho^2(z)]. \tag{2}$$

Choosing the expected value, $E[\ ]$, to be a simple integral average, we obtain

$$\lambda = \left(\frac{1}{L}\right)\int_0^L g(z)\frac{\left[\int_0^l f(z,x)\phi(x)\,\mathrm{d}x\right]^2}{\int_0^l \phi^2(x)\,\mathrm{d}x}\,\mathrm{d}z \tag{3}$$

where the realization index z ranges from 0 to L.

To determine the function ϕ which maximizes λ, we proceed by applying the usual calculus of variations. This is done by perturbing the function ϕ by the small amount $\varepsilon\delta\phi$ (see for example, Panofsky and Dutton, 1984). Replacing $\phi(x)$ in (3) with the perturbed value

$$\phi(x) + \varepsilon\delta\phi(x)$$

and taking the limit

$$\left.\frac{\mathrm{d}\lambda(\varepsilon)}{\mathrm{d}\varepsilon}\right|_{\varepsilon\to 0} = 0,$$

we obtain an additional constraint on ϕ which will eventually allow quantitative determination of ϕ. After considerable algebra, we obtain

$$\int \tilde{K}(x,y)\phi(y)\,\mathrm{d}y = \lambda\phi(x) \tag{4}$$

$$\tilde{K}(x,y) = \frac{1}{L}\int_0^L g(z)f(z,x)f(z,y)\,\mathrm{d}z, \tag{5}$$

where x and y are two different relative positions within the realization. $\tilde{K}(x,y)$ is simply the usual covariance matrix transformed by the weighting function $g(z)$. This result (4–5) allows use of the usual mathematics for solution of the eigenvalue-problem. All of the convenient properties of eigenvectors follow. For application to actual data (Busch and Petersen, 1971), we must apply the discrete version of (5) in which case z, $g(z)$, and $f(z,x)$ become discrete variables determined by the data resolution.

While the eigenvector-decomposition reveals more information than is possible with the composited structure of samples, it must be remembered that it represents a decomposition which optimizes variance explained and does not necessarily represent an optimum physical decomposition. For example, in the process of maximizing the variance, the first eigenvector may represent a compromise between two actual physical modes. This physical ambiguity might be reduced by rotating the eigenvectors (e.g., Richman, 1983) which was not carried out here.

3. Weighting functions

In practice the weighting function $g(z)$ applied to each potential sample can be chosen to represent any particular feature of the flow. As one example, $g(z)$ can be chosen to emphasize bursts of small scale activity defined by the Variable Interval Time Averaging (VITA) technique (e.g., Chen and Blackwelder, 1978; Schols, 1984). Some other examples are now noted.

3.1. Unweighted

For perspective, consider the case of constant weighting function

$$g(z) = 1, \tag{6}$$

where all potential samples are accepted equally without differentiation between samples. If $f(z, x)$ is univariate and samples are collected by moving a sample rake (Fig. 1a) sequentially through a homogeneous record, then the resulting correlation matrix is approximately persymmetric. That is, all elements in any given diagonal of the matrix are approximately equal except for the small undesired influence of the boundaries of the finite record. Then

$$\tilde{K}(x, y) \simeq \tilde{K}(x - y) \tag{7}$$

and the eigenvectors approach Fourier modes regardless of the structure of motions leading to the correlation where x and y are two relative positions within the sample. If $f(z, x)$ is multivariate corresponding to "stacking" of variables (Fig. 2), then only submatrices are persymmetric and some phase information is retained. The off-diagonal submatrices are the cross-correlation matrices and contain the phase information while the diagonal submatrices are the autocorrelation matrices. Since each submatrix is essentially persymmetric and can be reduced to a single function, the entire correlation matrix still contains only limited information on the multivariate structure (Frank, 1986).

The application of the weighting function eliminates this particular sampling problem (8). The weighting function emphasizes samples

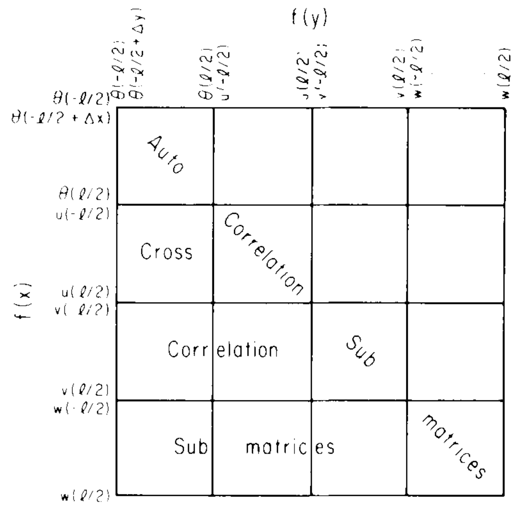

Fig. 2. Lagged multivariate covariance matrix for the present study of aircraft records. $f(x)$ is the multivariate observational vector consisting of temperature and the three velocity components. x and y are relative positions within each sample of width l.

where the desired event is centered in the sample window. The values of $f(z, x)$ are then no longer stationary with respect to relative position in the sample rake and phase information is captured.

3.2. Flux criteria

Specification of the weighting function does not require any knowledge of the shape or structure of the target motions and can be related to a consequence of the turbulence. For example, we can ask; what is the nature of the motions most responsible for the vertical flux of variable ψ? Then we specify the weighting function to be the vertical flux

$$g(z) = \frac{2}{N_{\delta x}} \sum w(z, x)\, \psi(z, x), \quad -\delta x \leqslant x \leqslant \delta x, \tag{8}$$

where $N_{\delta x}$ is the number of points in the weighting region, δx is the half width of the weighting region, as in the example in Fig. 1, and $w(z, x)$ is the vertical motion. Both $w(z, x)$ and $\psi(z, x)$ may be part of a multivariate observational vector $f(z, x)$. With this weighting function, the samples could be divided into two groups according to the sign of the flux of each sample.

3.3. Microfronts

The weighting function can be constructed by evaluating the similarity of the sample to an indicator function $h(x)$ which might be chosen in terms of a suspected reoccurring feature of the flow. For example, to study eddy microfronts, the horizontal changes of variable $\psi(z,x)$ can be emphasized by specifying the indicator function to be a step function (Fig. 1b)

$$h(x) = \left(\frac{2}{N_{\delta x}}\right)\begin{cases} 1: & 0 < x < \delta x \\ -1: & -\delta x < x < 0. \end{cases} \tag{9}$$

The weighting function is then determined as

$$g(z) = \sum_x h(x)\,\psi(z,x), \tag{10}$$

so that samples with horizontal structure of $\psi(z,x)$ most similar to the step function will be weighted the most. This weighting function is proportional to the difference of the values of $\psi(z,x)$ averaged over distance δx on each side of the sample center $x = 0$, and thus emphasizes samples with concentrated gradients at the sample center. Note that determination of the weighting function in terms of more than one variable is not desirable since it would act to suppress phase differences between variables.

3.4. Conditional sampling

The weighting function reduces to conditional sampling by assigning it a value of zero or one depending on whether the original weighting-function exceeds a critical value CV.

$$g(z) = \begin{cases} 1: & g(z) > \mathrm{CV} \\ 0: & g(z) < \mathrm{CV}. \end{cases} \tag{11}$$

That is, samples are selected only when the weighting function exceeds the critical value. All other samples are discarded. Samples may still be collected separately for each sign of the original weighting function. Since several samples of the same event may be inadvertently selected, overlap criteria are applied. For example, with the conditional sampling applied in Sections 5, 6, we will choose the sample with the largest value of $g(z)$ subject to the constraint that samples selected by (11) do not overlap.

Results from conditional sampling are based on a limited number of samples which in turn depend on the choice of the critical value CV. As a consequence, such results are not as unique compared to continuous weighting which does not require specification of a critical value and includes all of the events in the record. The results based on conditional sampling are sharper in that the ensemble of samples contain only one centered "picture" of each event and contain only the strongest events. However, the sample size is often limited to the extent that results based on conditional sampling are contaminated by noise. Results based on continuous weighting are less vulnerable to noise as can be shown with analysis of artificial turbulence (not reported here) and as will be evident from the analyses in Sections 5 and 6. With artificial turbulence consisting of simple building blocks and high amplitude white noise, conditional sampling was unable to extract the basic building block while use of continuous weighting produced a smoothed version of the building block.

While the continuous weighting does not require selection cutoff criteria and is less sensitive to noise, it includes uncentered samples of the events or samples of weak events. With sequential sampling in a time series (Fig. 1a), the method captures many "pictures" of the same event as the sampling window moves past the event. The most weighted "picture" will be that one where the event is centered; none-the-less, the composite picture and eigenvectors are somewhat fuzzy and some details may be missing. By raising the right-hand side of (10) to a power higher than one, the results become sharper but more vulnerable to noise.

3.5. Present study

In the present study, both conditional sampling and continuous weighting will be applied. Multivariate samples of the horizontal structure of temperature and the three wind components are collected. To study microfronts we will express the weighting function in terms of the horizontal gradient of the vertical velocity using the step indicator function (9–10). Temperature is not as useful since in stratified flows, strong horizontal temperature gradients sometimes occur at dynamically inactive locations. The horizontal velocity components are more contaminated by larger scale motions. The use of gradients of vertical motion instead of the vertical motion itself is not only of interest for the study of microfonts but also reduces the influence of trend. Then additional filtering is not required, although specification of the width of the sampling rake (Fig. 1a) and choice of $g(z)$ can be viewed as a filter. The weighting function will be evaluated over distance δx, chosen to be smaller than the width of the samples, l, in order to include the structure of the environmental flow surrounding the event of interest. The sampling rake in the present study will consist of twenty teeth, each separated by distance $\Delta x = \frac{1}{19} l$ (Fig. 1). To generate potential samples, the sampling rake is sequentially moved through the record distance Δx between each sample collection allowing considerable overlap between samples.

The application of the weighting and sample selection criteria to only one variable of the multivariate observational vector, and then only to a subregion of the sampling rake, allows assessment of the impact of noise. The sampling process can generate artificial coherence from noise for vertical motion within the weighted region. However such artificial structure would not explain coherence involving other variables or coherence of vertical motion outside the weighting region.

4. Aircraft data

This study examines turbulence data collected with fast-response instruments mounted on aircraft in the Alpine Experiment (ALPEX) and in the Severe Environmental Storms and Mesoscale Experiment (SESAME). We will analyze the record of strongest turbulence in the bora of 6 March 1982 over the coastal range of Northern Yugoslavia (Mahrt and Gamage, 1987; leg V2, their Fig. 3) where drafts reach relative vertical velocities of 10 m/s. This record is about 40 km long. The SESAME aircraft data (Mahrt, 1985) was collected in nocturnal boundary layers during a synoptically quiet period. We will analyze data collected in weak intermittent turbulence at the top of a strongly stratified surface inversion layer in the early morning of 5 May 1979. Turbulence within the underlying surface inversion is suppressed by the strong stratification. This data consists of six flight legs about 15 km long.

Four variables, potential temperature and the three velocity components, are "stacked" into the observational vector (Fig. 2) which in terms of relative position x is of the form

$$f(x) = [\theta(-l/2), \theta(-l/2 + \Delta x) \ldots \theta(l/2), u(-l/2) \ldots u(l/2), v(-l/2) \ldots v(l/2), w(-l/2) \ldots w(l/2)]. \qquad (12)$$

Stacking of variables has been previously adopted by Kutzbach (1967), Petersen (1976), and Barnett (1983) and can identify simultaneous coherence between more than two variables, not possible with spectral decomposition.

The mean of each variable is removed separately for each sample so that the covariance is due to structure within each sample without the influence of variance between sample means. We will not scale with the sample standard deviation in order to preserve the importance of high amplitude structures. Instead the calculation of the lagged correlation matrix is equivalent to scaling with the standard deviation due to the variation of horizontal structure between the demeaned weighted samples.

For conditional sampling, the critical values (CV in eq. 11) for the vertical motion change are chosen to extract at least 25 of the strongest events. These nonoverlapping samples will account for more than half of the entire record. The sample widths are chosen as 912 m for the bora flow and 608 m for the nocturnal boundary layer. The sampling rake (Fig. 1) consists of 20 teeth spaced every eight observational points corresponding to a rake resolution Δx of 48 m in the bora flow and 32 m in the nocturnal boundary layer. The subsequent stacking of variables leads to a 80×80 lagged correlation matrix. The weighting function is computed from all of the observational points in a centered subregion of 384 m for the bora and 256 m in the nocturnal boundary layer.

5. Draft frontal structures in strong bora turbulence

We first analyze results obtained from the conditional sampling procedure (11) based on the weighting function (10) evaluated in terms of the indicator function (9). Recall that the indicator function is designed to identify regions with sharp horizontal gradients of vertical motion. In the bora turbulence, the conditional sampling selects almost exclusively edges of strong drafts. Since the mean horizontal momentum decreases with height, the updrafts are generally moving horizontally faster than the surrounding ambient flow, while the downdrafts move slower. The draft "upstream" edge is the location where the relative horizontal motion of the draft converges with the slower ambient flow (expected location of the front). The aircraft data allows computation of the convergence of only the flow component parallel to the flight track which will hereafter be referred to as simply the convergence. For brevity we will examine mainly the fronts or draft-upstream edges. The composite structure and eigenvectors for the draft-downstream edges tend to be less defined as is also suggested by the skewness of the structure function (Mahrt and Gamage, 1987).

We first consider the case of strongest bora turbulence. The mean shear is variable but tends to be directed northeastward along the flight track (Mahrt and Gamage, 1987; their Fig. 15). A small shear component directed perpendicular to the flight track also seems likely. We will refer to the horizontal wind component in the flight direction as the along-flight component (here northeastward) while the horizontal component perpendicular to flight direction will be referred to as the crosswind component (here northwestward).

To obtain an overall impression, we first examine the composited structures (Fig. 3). As expected, results based on continuous weighting are less vulnerable to noise but fail to capture the sharpness of the microfront. Nonetheless the multivariate structure based on conditional sampling qualitatively agrees with that based on continuous weighting for the composited data and the first few eigenvectors. The eddy frontal zone of strong horizontal shear of the vertical velocity is located at the center of Fig. 3 (approximately 450 m). The vertical heat flux for the composited structure is downward as expected with the stable stratification even if weak.* The systematic structure for the horizontal motion perpendicular to the flight track is apparently due to the small component of the mean shear perpendicular to the flight.

All of the features of the composite variations are not associated with a single type or phase of the coherent structures as is shown by the eigenvector decomposition. The individual eigenvectors for the cases considered here never explain more than 25% of the variance since the motion is fully turbulent and, therefore, quite complex.

The leading eigenvector (Figs. 3, 4) corresponds to downward heat flux and explains 22% of the variance of the conditionally selected samples. Note that this eigenvector is less noisy than the composited structure and corresponds to somewhat larger horizontal scale; that is, the eigenvector calculation maximizes the coherence (lagged covariance). In contrast, the composited structure suffers from interference between different modes.

The front, as represented by the first eigenvector, is characterized by relatively sharp horizontal changes of vertical velocity and temperature. For many of the individual samples, the horizontal changes of temperature and vertical motion at the front are sharper than the changes based on conditional sampling and almost always sharper than the results based on continuous weighting. The vertical motion and along flight flow of the first eigenvector at the microfront (Fig. 7) is consistent with a transverse vortex (horizontal vorticity vector perpendicular to the shear) which is tilted with respect to the horizontal plane. Longitudinal vortices cannot be

* The amplitude of the composite temperature variation is small because the strong turbulence has reduced the strength of the stratification and also because some of the samples contain horizontal temperature gradients of opposite sign to that of the composited structure. It should be noted that the eigenvectors describe the horizontal structure of the relative flow based on samples with the horizontal average removed. As a result, it is not possible to unambiguously determine whether the shear at the microfront is primarily the edge of one eddy circulation or a shear zone between two eddy circulations. To be consistent with eq. (5), the composite for continuous weighting is computed as

$$\bar{f}(x) = [\overline{|g(z)|^{1/2}}]^{-1}(1/N) \sum_{z=1}^{N} |g(z)|^{1/2} f(x, z),$$

where

$$\overline{|g(z)|^{1/2}} \equiv (1/N) \sum_{z=1}^{N} |g(z)|^{1/2},$$

and N is the number of samples.

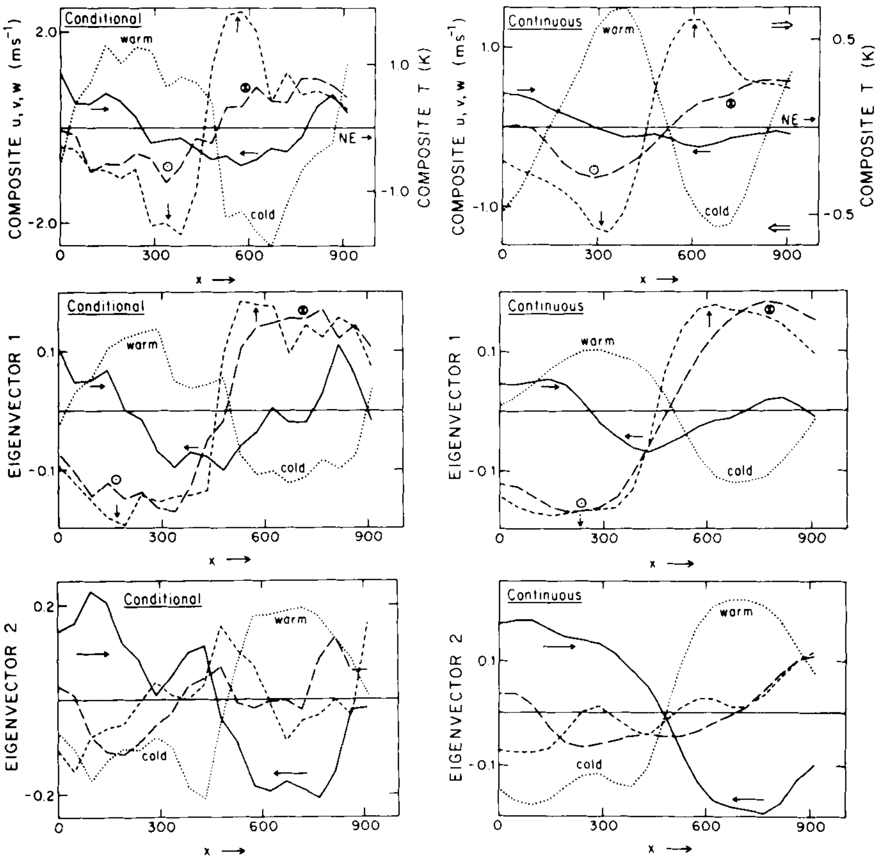

Fig. 3. Composite structure and leading eigenvectors of the relative flow for the strong turbulence case for vertical motion (short dash), horizontal motion along the flight track (solid) positive to the right (northeastward), horizontal motion perpendicular to the flight track (long dash) positive into paper (northwestward), and temperature (dotted). Direction of along flight and vertical flow components are also noted with arrows while the direction of the cross flow is indicated with the usual symbols ⊗ and ⊙ indicating flow into and out of paper, respectively. Double arrows indicate relative direction of overlying mean flow (upper arrow) and underlying mean flow (lower arrow).

easily observed with this data since the phase lines would be roughly parallel to the flight path.

The relative horizontal motion at the front is directed southwestward associated with horizontal divergence of the updraft. In the composited structure, the maximum southwestward momentum occurs behind the microfront in the updraft region suggesting upward transport of horizontal momentum from the underlying southwestward bora flow. If the heat flux is used to compute the weighting function as outlined in Subsection 3.2, then the relative southwestward momentum is even more developed in the updraft region behind the front (northeastward of the front) but still extends ahead of the front.

The extension of southwestward momentum ahead of the microfront could be associated with a pressure head or positive pressure perturbation at the front due to the relative horizontal motion of the draft through the ambient flow. Such a pressure perturbation has been previously used to explain the momentum field around convective drafts (Newton and Newton, 1959; Mahrt, 1981; and others). In fact, it might be possible to consider the accelerated mass ahead of the microfront as additional virtual mass of the draft similar to treatments in Lamb (1932).

The second eigenvector which explains 14% of the variance of the conditionally selected samples, corresponds to horizontal convergence

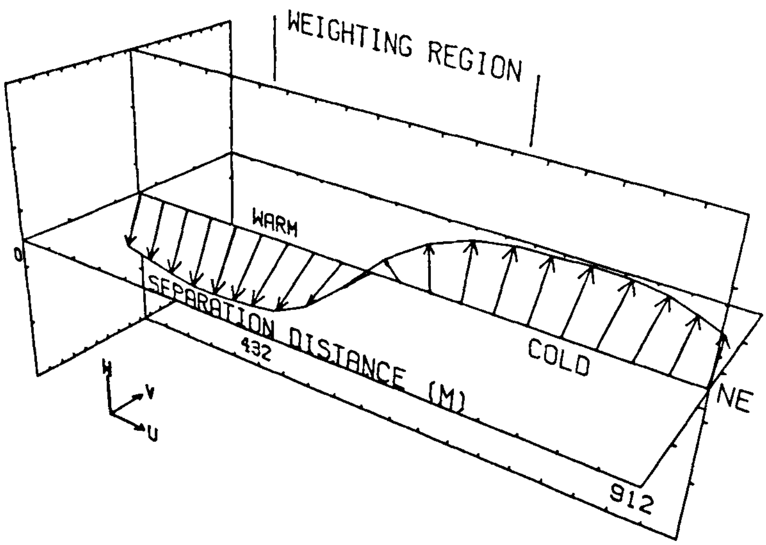

Fig. 4. Three-dimensional plot of airflow for the strong bora turbulence as captured by the first eigenvector based on continuous weighting.

(deceleration of the along flight motion) and a decrease of temperature across the front with little structure in the vertical and cross velocity components. The structure is most obvious for continuous weighting while the eigen structure for conditional sampling is partially obscured by noise. This negative correlation between temperature and along flight motion (northeastward) is counter to the correlation which would be produced by down-gradient vertical mixing (transport from high values to low values). The structure of the second eigenvector is consistent with a second phase of shear-driven overturning where the perturbation motion curves back against the mean flow (Fig. 5).

The third eigenvector (not shown) explains 10% of the total variance of the conditionally selected samples and corresponds to significant upward heat flux probably corresponding to the rebounding stage. In this stage, displaced air is accelerated back towards the buoyancy equilibrium level by buoyancy and perhaps the eddy pressure field. If the first eigenvector represents the first stage of overturning where the vertical transfer is down-gradient, then the first three eigenvectors could represent sequential stages of overturning motion (Fig. 5).

This discussion is somewhat oversimplified in that two or more eigenvectors are simultaneously

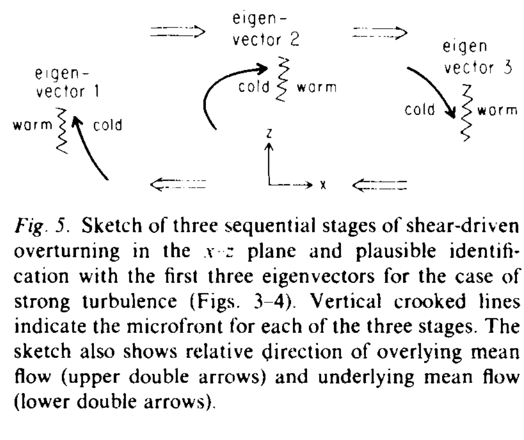

Fig. 5. Sketch of three sequential stages of shear-driven overturning in the x–z plane and plausible identification with the first three eigenvectors for the case of strong turbulence (Figs. 3–4). Vertical crooked lines indicate the microfront for each of the three stages. The sketch also shows relative direction of overlying mean flow (upper double arrows) and underlying mean flow (lower double arrows).

important for many of the samples. Furthermore, the second and third eigenvectors can occur with either sign of the expansion coefficient.

Higher number eigenvectors based on conditional sampling become progressively noisier for all four variables. The higher modes are probably not significant becuase of the small sample size of 25 events. In fact, the significance of the leading few eigenvectors is not known with certainty. Relaxing the cutoff criteria allows more samples but does not significantly reduce the noise. The higher number eigenvectors with continuous weighting show more spatial coherence. The fourth and fifth eigen modes show coherent, smaller-scale events where the heat transport is downward but the phase of the horizontal velocity components are altered compared to lower order eigenvectors.

Some features of the results from conditional sampling are not present with continuous weighting. For example in the first eigenvector based on conditional sampling, a secondary temperature front occurs at the convergence zone ahead (southeastward) of the microfront. This secondary front does not appear with continuous weighting and might therefore be considered insignificant.

As an additional check on the significance of the eigenvectors, we analyzed a second aircraft leg implemented 300 m higher in the same field of strong turbulence. The three leading eigenvectors from this record (not shown) exhibited similar properties to the above decomposition. For example the eigenvector representing a strong change of vertical velocity represents down-gradient vertical transfer while the other leading eigenvector is associated with strong temperature change, reversed along flight momentum and weak vertical motion. Again a third eigenvector leads to significant upward heat flux.

In general, the eigenvectors become noisier when the width of the weighting region is decreased and become smoother when the weighting region is increased. Expressing the weighting function in terms of other variables, such as temperature or horizontal motion, changes some aspects of the resulting eigenvectors.

6. Microfront structure in intermittent stratified turbulence

For comparison we briefly consider the case of relatively weak intermittent patches of turbulence occurring near the top of a strong nocturnal surface inversion layer. To interpret the eigenvector structure, we note that the intermittent turbulence is generated by shear between cold southeastward flow and overlying warm northwestward flow.

The first three eigenvectors for continuous weighting are shown in Fig. 6. The first eigenvector, which explains 24% of the variance, corresponds to the crossing of an interface

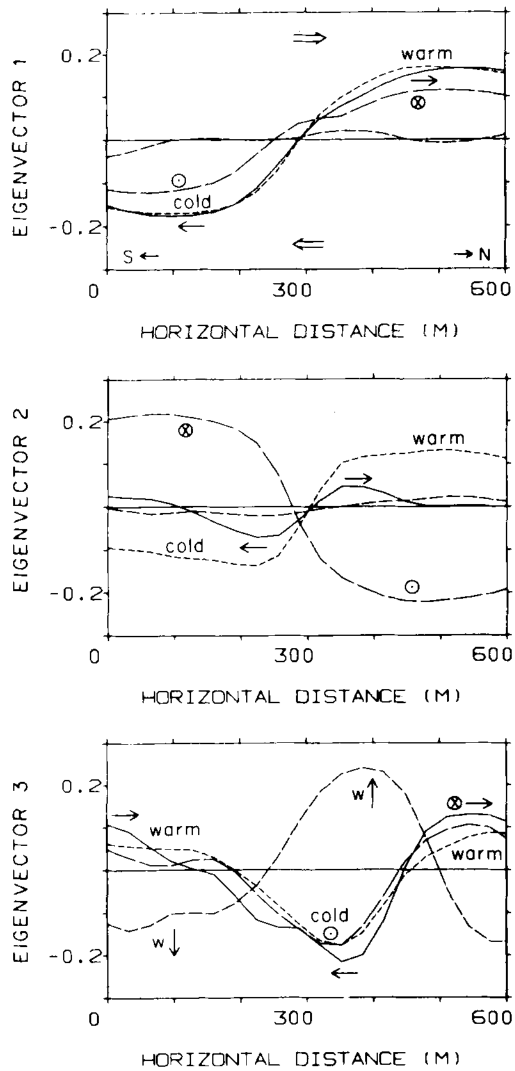

Fig. 6. Leading eigenvectors for the case of weak intermittent turbulence based on continuous weighting for vertical motion (intermediate dash), horizontal motion along the flight track (solid) positive to the right (northward), horizontal motion perpendicular to the flight track (long dash) positive into paper (toward the west), and temperature (short dash). Direction of along flight and vertical flow components are also noted with arrows while the direction of the cross flow is indicated with the usual symbols ⊗ and ⊙ indicating flow into and out of paper, respectively. Double arrows indicate relative direction of overlying mean flow (upper arrow) and underlying mean flow (lower arrow).

between cold southeastward flow and warm northwestward flow. Note that vertical motion is unimportant even though the samples used to compute the covariance matrix were weighted according to the vertical motion structure. That is, the vertical motion is not the most important factor in terms of explaining the horizontal coherence even though the most weighted samples contain significant horizontal change of the vertical velocity at the sample center. More specifically, the occurrence and strength of the horizontal structure represented by the first eigenvector is not correlated with the strength of the horizontal shear of vertical velocity. Apparently, the first eigenvector can identify the most important structure even though the weighting function is not particularly relevant. Results were recalculated with the indicator function applied to temperature instead of vertical motion. The resulting eigen modes are quite similar with only a slight increase of variance explained. The first eigenvector based on conditional sampling is nearly the same as that based on continuous weighting except noisier.

The unimportance of vertical motion probably indicates the importance of two-dimensional horizontal vortical modes (e.g., Riley et al., 1981; Lilly, 1983) which result from suppression of vertical motion by the stratification. Such a possibility is further supported by the second eigenvector (13% of the variance) where vertical motion remains unimportant and the direction of the horizontal flow is rotated from the direction of the first eigenvector. The first two eigenvectors in concert can describe horizontal rotation of the wind vector or horizontal meandering.

The third eigenvector (10% of the variance) corresponds to down-gradient transfer which is expected in regions of active turbulence (Figs. 6, 7). With conditional sampling, this eigenvector becomes the second most important one. With this eigenvector, a microfront zone occurs in a pulse of rising cold air towards the southeast (direction of the cold air flow within the underlying surface inversion layer). The southeastward momentum at the microfront is probably due to vertical advection of momentum and horizontal divergence due to vertical deceleration of the negatively buoyant updraft. This surge of cold air is a part of the circulation which then sinks back down into the inversion layer along with warmer sinking air (Fig. 7). The expansion coefficient for this eigenvector (inner product of eigenvector and observational vector) also occurs with negative values in which case the microfront occurs at the leading edge of warm sinking flow directed toward the northwest.

The fourth and fifth eigenvectors show properties similar to simple gravity waves in that vertical motion is out of phase with temperature

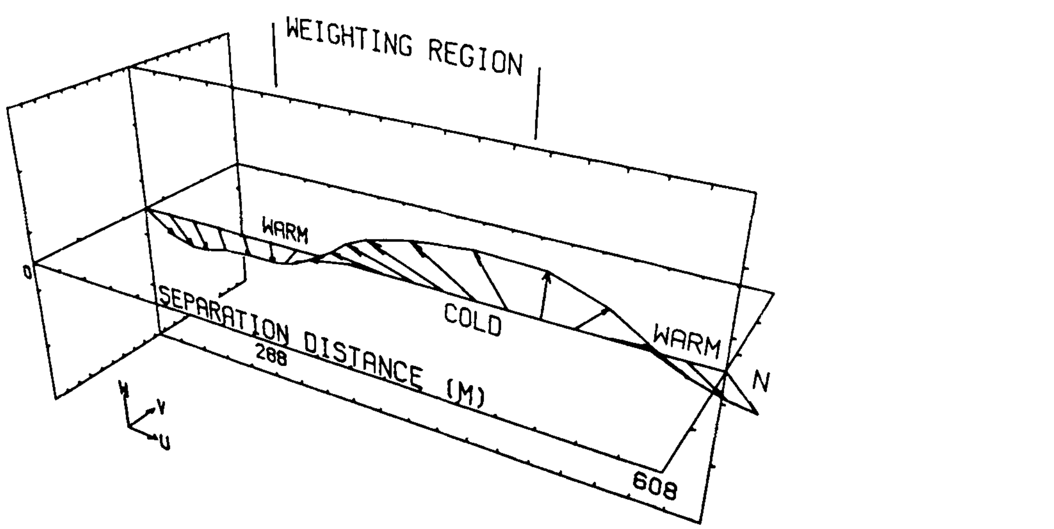

Fig. 7. Three-dimensional plot of airflow for the weak turbulence as captured by the third eigenvector for continuous weighting.

and horizontal motion by about $\frac{1}{4}$ of a length scale. The original records seem to indicate considerable gravity wave activity. Horizontal modes in the present analysis are more predominant than gravity waves. This is consistent with the hypothesis that the horizontal modes result from the decay of the three-dimensional turbulence. Gravity waves initiated by the patches of turbulence apparently propagate away from the turbulence regions. The importance of temperature in the multivariate coherence for the horizontal modes may reflect the influence of previous turbulent vertical mixing even though vertical motion is no longer correlated with the structure of the other variables.

7. Conclusions

The present study has examined narrow zones of strong horizontal shear and temperature gradients referred to as eddy microfronts. In the case of the strong turbulence examined here, the first eigenvector of the lagged covariance matrix corresponds to expected down-gradient transfer of heat and horizontal momentum. The second eigenvector represents an opposite correlation between temperature gradients and horizontal momentum in such a way to be consistent with a second stage shear-driven overturning where the perturbation flow curves back against the mean flow. The third eigenvector represents upward buoyancy flux as would be produced by the acceleration of displaced fluid back towards its buoyancy equilibrium level. These three eigenvectors are consistent with sequential stages of shear-driven overturning although the geometric limitations of aircraft data prevent conclusive examination.

For the case of weak intermittent turbulence in strongly stratified flow, the leading two eigenvectors correspond to two-dimensional horizontal modes. These modes have distinct temperature structure. The three-dimensional turbulent eddies (third eigenvector) coexist with these modes and some gravity wave activity (higher order eigenvectors). The generality of these results are not known.

The vertical structure of the horizontal two-dimensional modes could not be examined here. It may be that such horizontal modes move somewhat independently at different levels leading to enhanced vertical shear and local development of turbulence. Such intermittent turbulence might generate significant vertical transport even if the Richardson number of the averaged flow is not small. Such a possibility could account for the fact that sampling of intermittent turbulence based on gradients of vertical velocity found important horizontal modes. Such horizontal modes may also lead directly to horizontal diffusion which cannot be studied with aircraft data.

The above results are based partly on computation of the eigenvectors of the lagged, multivariate covariance matrix constructed from samples of microfronts extracted by conditional sampling. The eigenvectors revealed important information about the structure of the eddy frontal regions that was not obvious from examination of the composited structure.

A new technique has been developed for computing the eigenvectors from the original record which does not require formulation of a set of sampling criteria as needed in conditional sampling. This technique uses a weighting function which can be formulated without the degree of a priori commitment needed for conditional sampling. As a result, this method is particularly useful for the initial study of flows where not enough is known about the dominant eddies to intelligently construct absolute sampling criteria. With such continuous weighting, the eigenvectors show greater coherence, particularly the higher order eigenvectors. Such calculations are less vulnerable to noise at the expense of some loss of structural detail. If desired, the dependence of the results on the initial choice of the indicator function (9) can be reduced by iterating where the indicator function is chosen to be the first eigen of the previous iteration.

8. Acknowledgements

We gratefully acknowledge the comments of D. K. Lilly, Nimal Gamage, and Paul Ruscher and the computational assistance of Wayne Gibson. This material is based upon work supported by the Global Atmospheric Program and the Meteorology programs of the National Science Foundation under Grants ATM-8518461 and ATM-8521349. The National Center for Atmospheric Research is acknowledged for computer resources and for the use of the Queen Air research aircraft in SESAME and the Electra aircraft in ALPEX.

REFERENCES

Antonia, R. A. and Van Atta, C. W. 1978. Structure functions of temperature fluctuations in turbulent shear flows. *J. Fluid Mech. 84*, 561–580.

Antonia, R. A., Chambers, A. J., Friehe, C. A. and Van Atta, C. W. 1979. Temperature ramps in the atmospheric surface layer. *J. Atmos. Sci. 36*, 99–108.

Barnett, T. P. 1983. Interaction of the monsoon and Pacific Trade wind system at interannual time scales. Part I: The equatorial band. *Mon. Wea. Rev. 111*, 756–773.

Blackwelder, R. F. and Kaplan, R. E. 1976. On the wall structure of the turbulent boundary layer. *J. Fluid Mech. 76*, 89–112.

Brown, G. L. and Thomas, S. W. 1977. Large structure in a turbulent boundary layer. *Phys. Fluids 20*, S243–S252.

Busch, N. and Petersen, E. L. 1971. Analysis of nonstationary ensembles. *Statistical Methods and Instrumentation on Geophysics*. Teknologisk Forlag, Oslo, Norway, 71–92.

Chen, C.-H. P. and Blackwelder, R. F. 1978. Large-scale motion in turbulent boundary layer: A study using temperature contamination. *J. Fluid Mech. 89*, 1–31.

Frank, H. 1986. Masters Thesis, Department of Atmospheric Sciences, Oregon State University, Corvallis, Oregon, U.S.A.

Gibson, C. H., Chen, C. C. and Lin, S. C. 1968. Measurements of turbulent velocity and temperature fluctuations in the wake of a sphere. *AIAA J. 6*, 642–649.

Greenhut, G. K. and Khalsa, S. J. S. 1982. Updraft and downdraft events in the atmospheric boundary layer over the Equatorial Pacific Ocean. *J. Atmos. Sci. 39*, 1803–1818.

Kaimal, J. C. and Businger, J. A. 1970. Case studies of a convective plume and a dust devil. *J. Appl. Meteorol. 9*, 612–620.

Kim, H. T., Kline, S. J. and Reynolds, W. C. 1971. The production of turbulence near a smooth wall in a turbulent boundary layer. *J. Fluid Mech. 50*, 133–160.

Kutzbach, J. E. 1967. Empirical eigenvectors of sea level pressure, surface temperature and precipitation complexes over North America. *J. Appl. Meteorol. 6*, 791–802.

Lamb, H. 1932. *Hydrodynamics*. Cambridge, 738 pp.

Laufer, J. 1975. New trends in experimental turbulence research. *Annual Rev. Fluid Mech. 7*, 307–326.

Lilly, D. K. 1983. Stratified turbulence and the mesoscale variability of the atmosphere. *J. Atmos. Sci. 40*, 749–761.

Lumley, J. L. 1970. *Stochastic tools in turbulence*. Academic Press, New York, 194 pp.

Mahrt, L. 1985. Vertical structure and turbulence in the very stable boundary layer. *J. Atmos. Sci. 42*, 2333–2349.

Mahrt, L. 1981. Circulations in a sheared inversion layer at the mixed layer top. *J. Meteorol. Soc. Japan 59*, 238–241.

Mahrt, L. and Gamage, N. 1987. Observations of turbulence in stratified flow. *J. Atmos. Sci. 44*, 1106–1121.

Newton, C. W. and Newton, H. R. 1959. Dynamical interactions between large convective clouds and environment with vertical shear. *J. Meteorol. 16*, 483–496.

Panofsky, H. A. and Dutton, J. A. 1984. *Atmospheric turbulence* (ch. 12). John Wiley and Sons, 397 pp.

Petersen, E. L. 1976. A model for the simulation of atmospheric turbulence. *J. Appl. Meteorol. 15*, 571–587.

Richman, M. B. 1983. Rotation of principal components. *J. Climatol. 6*, 293–335.

Riley, J. J., Metcalfe, R. W. and Weissman, M. A. 1981. Direct numerical simulations of homogeneous turbulence in density-stratified fluids. *Proc. AIP Conf. Nonlinear Properties of Internal Waves*, Bruce J. West, Ed., Am. Institute of Physics, New York, 79–112.

Schols, J. L. J. 1984. The detection and measurement of turbulent structures in the atmospheric surface layer. *Bound.-Layer Meteorol. 29*, 39–58.

Schols, J. L. J. and Wartena, L. 1986. A dynamical description of turbulent structures in the near neutral atmospheric surface layer: The role of static pressure fluctuations. *Bound.-Layer Meteorol. 34*, 1–15.

Townsend, A. A. 1976. *The Structure of Turbulent Shear Flow*, Chapter 1. Cambridge University Press, 429 pp.

Wilczak, J. M. 1984. Large scale eddies in the unstable atmospheric surface layer. *J. Atmos. Sci. 41*, 3537–3550.